

Article

# Analyzing the Design and Performance of a DC Linear Stepper Motor

Monier Habil <sup>1,\*</sup> , Fatih Anayi <sup>1</sup>, Yiqin Xue <sup>1</sup> and Khalefa Alnagasa <sup>2</sup>

<sup>1</sup> Wolfson Centre for Magnetics, School of Engineering, Cardiff University, Cardiff CF24 3AA, UK; anayi@cardiff.ac.uk (F.A.); xue@cardiff.ac.uk (Y.X.)

<sup>2</sup> Faculty of Information Technology Engineering, Union Nikola Tesla University, 11000 Belgrade, Serbia; khalefa.alnagasa@yahoo.com

\* Correspondence: habilmm@cardiff.ac.uk; Tel.: +44-7479764322

**Abstract:** This paper describes the design and modelling of a DC linear stepper motor (DLSM), to investigate the air-gap magnetic flux density and the static features of the thrust force under the DC current excitation condition, while taking the nonlinear properties of iron materials used into account. A Finite Element Method (FEM) study utilizing software called a “MagNet” was employed to model and construct a linear DC motor. The thrust force, air-gap flux density, and static thrust force at various airgaps were compared in simulation and real time. The result showed that the magnetic flux density presents a sinusoidal shape in both the simulation and measurement, where the peak error value was around 7.14%. A comparison was made with thrust force, as the armature current has different values; the results show that the difference between the experimental and computed peak value was 8.07%, while the error between the measured and simulated value was 5.02% when the thrust force was measured at different air gap lengths.

**Keywords:** linear stepper motor; moving magnet linear motors; magnetic flux density; “MagNet” software



**Citation:** Habil, M.; Anayi, F.; Xue, Y.; Alnagasa, K. Analyzing the Design and Performance of a DC Linear Stepper Motor. *Machines* **2023**, *11*, 785. <https://doi.org/10.3390/machines11080785>

Academic Editor: Parviz Famouri

Received: 12 June 2023

Revised: 24 July 2023

Accepted: 27 July 2023

Published: 29 July 2023



**Copyright:** © 2023 by the authors. Licensee MDPI, Basel, Switzerland. This article is an open access article distributed under the terms and conditions of the Creative Commons Attribution (CC BY) license (<https://creativecommons.org/licenses/by/4.0/>).

## 1. Introduction

In recent years, the demand for high-performance linear motion systems has been on the rise in various industrial and commercial applications [1]. Linear motors, known for their precise control, high acceleration capabilities, and absence of mechanical wear, have emerged as a promising solution to meet these demands. Among the different types of linear motors, the DC linear stepper motor has attracted substantial attention due to its unique design and improved performance characteristics [2].

Linear motors provide a direct linear motion without the need for mechanical transmission devices, such as gears, belts, chains, or motor couplings. This compliance eliminates backlash, reduces friction, and increases motor efficiency, unlike conventional rotary motors [3,4]. The simple structure of DLSM offers high flexibility to the machine in terms of size and space, with the few components needed in the motor and limited lubrication making installation and maintenance easy. Due to linear machines’ advantages in delivering precise linear motion and accurate positioning, they have found widespread use in various industries for applications requiring the precise control of linear motion [5]. DC linear stepper motors are frequently employed in industrial automation systems, such as pick-and-place machines, material handling equipment, and robotic systems. They are also utilized in CNC machines, 3D printers, and transportation systems [6–8].

For linear motion applications, various linear motor configurations and technologies can be utilized [9]. The most frequently employed linear motors include induction linear motors, switched reluctance linear motors, and permanent magnet linear motors [10–12]. Among these options, permanent magnet linear motors are deemed to be most suitable for linear motion functions due to their notably higher efficiency and greater power density [13].

Permanent magnet linear motors can be further considered as moving iron, moving magnet, and moving coil types. Each type has its own advantages and disadvantages depending on the practical usage scenario. Moving coil linear motors have a simple structure, but their wiring, which is wrapped around the moving part, can be less secure, and dissipating the generated heat can be challenging [9,14]. Moving iron linear motors are durable and inexpensive, but their primary weakness is their low efficiency. Recent research has been conducted on linear motors with moving magnets, and various configurations for various applications have been reported. These motors offer significant energy-saving benefits when compared to conventional systems that employ rotary motors and crank-driven mechanisms [15–17].

To assess the performance and electromagnetic characteristics of linear motors, it is crucial to have a precise understanding of the magnetic field distribution. The evaluation of magnetic field distribution can be ensured using both numerical and analytical methods [18]. Finite Element Analysis (FEA) is a prominent numerical method that offers the advantage of incorporating the nonlinear magnetic saturation of cores and the actual motor design geometry. The magnetic field is computed by FEA by solving the governing equations derived from Maxwell's equations [19]. In the case of a moving magnet linear motor, FEA was used to calculate static shaft forces for different armature positions [20]. Furthermore, a comparison of key performance indicators was made between a moving magnet linear motor and a moving iron motor in [21]. FEA has proven useful in the optimization of the design of linear motors in previous studies [22].

The purpose of this paper is to present a thorough analysis of the design and construction of a DC stepper linear motor. Optimizing the motor's performance parameters, such as thrust force, airgap, and magnetic flux density, while ensuring a reliable and seamless operation is the primary objective. To accomplish this, both numerical simulations and experimental validations will be utilized.

The design process will involve selecting appropriate magnetic materials, determining optimal winding configurations, and optimizing the motor's geometry to achieve the desired performance characteristics. Furthermore, the effects of various parameters, such as air-gap length and armature current, will be thoroughly investigated to understand their influence on the motor's behavior.

## 2. Principle and Operation Analysis of DLSM

The fundamental operation of a DC linear motor is comparable to that of a conventional DC motor, but with a longer configuration. A linear motor converts electrical energy directly into linear mechanical motion, with no intermediate rotary-to-linear conversion mechanism required.

A DC linear motor is composed of a stator and an actuator (also known as a translator or armature). Typically, the stator consists of a series of magnets or electromagnets arrayed in a linear fashion. In contrast, the mover comprises a wire coil that interacts with the magnetic field produced by the stator [23,24].

The force production in a DC Linear stepper Motor (DCLSM) is based on the electrodynamic force principle. The force resulting from the interaction between the armature current and the magnetic flux provided by the permanent magnet is calculated using Lorentz's law  $F = iBL$ , which can be expressed as follows [25]:

$$F = I N B L \quad (1)$$

where  $F$  is the thrust generated in the motor, (Newtons,  $N$ ),  $I$  is the current flowing through the coil (Amperes,  $A$ ),  $B$  is the (Tesla,  $T$ ).  $L$  is the length of the coil perpendicular to the magnetic field (meters  $m$ ).

The thrust constant of the dc linear motor depends on the value of the magnetic flux density ( $B$ ), number of turns ( $N$ ) and coil current ( $I$ ). These parameters are fixed when the

motor is designed. Thus, the amount of current supplied to the coil can be adjusted to control the thrust produced by the motor. Motor thrust constant  $k_f$  is assumed to be:

$$k_t = N B L \quad (2)$$

By substituting Equation (2) into Equation (1), the final expression of thrust can be represented by:

$$F = k_t I \quad (3)$$

This implies that the motor's thrust constant,  $k_f$ , is proportional to the magnetic flux density in the air gap,  $B$ . The greater the magnetic flux density in the air gap,  $B$ , of the DLISM and  $k_f$  is the greater the motor's thrust constant [25].

The response of the mover in a DC Linear Stepper Motor (DLISM) is determined by calculating the mechanical time constant,  $T_m$ . This time constant enables us to determine how fast the mover can respond to system changes. Therefore, a reduced mechanical time constant ( $T_m$ ) indicates that the actuator can respond much more quickly [26,27]. A reduced  $T_m$  value indicates that the mover is capable of rapidly adjusting its position or speed in response to system changes or input signals. In applications where a fast and responsive mover is required, a lower mechanical time constant is optimal.

The mechanical time constant,  $T_m$  is calculated as follows:

$$T_m = \frac{MR}{k_t^2} \quad (4)$$

where  $T_m$  is the mechanical time constant,  $R$  is the coil resistance,  $M$  is the mover mass, and  $k_f$  is the thrust constant.

The mechanical time constant is the time at which the velocity of the mover reaches 62.3% of its utmost value [28].

Furthermore, the DC linear motor operates based on the principle of magnetic field interaction and electric current conversion, enabling the transformation of electrical energy into linear mechanical motion. Structurally, it consists of a stationary stator, comprising magnets or electromagnets, and a movable armature with coil windings [29]. By inducing magnetic fields through the stator and applying an electric current to the armature windings, the motor generates a force resulting from the interaction between these fields [29]. This force propels the armature along a predetermined linear path. Precise control of the motor's motion is achieved through the manipulation of the current direction and magnitude, employing commutation techniques. In summary, the DC linear motor effectively harnesses the principles of magnetic field interaction and electric current to facilitate a controlled linear motion [30,31].

The motor was chosen and developed as a DC linear stepper motor (DLISM). The mover consists of eight permanent magnet (NdFeB) blocks. The translator is designed to be double-sided (U sharp). Each side of the slider has four PMs, arranged as N-S-N-S. These PMs are split by three Tufnol blocks to isolate the permanent magnets, as seen in Figure 1. The back-iron is positioned in the field housing to complete the magnetic circuit produced by the permanent magnets. The armature core is constructed of a mild steel bar and built as a rectangular armature core. The field translator is placed within the carriage and moved with the help of linear bearings placed parallel to the length of the armature and fitted on aluminum rails. To investigate the impact that changing the air gap has on the motor's thrust, this model is built with an adjustable air gap. Table 1 shows the major characteristics and material specifications for the linear DC motor.

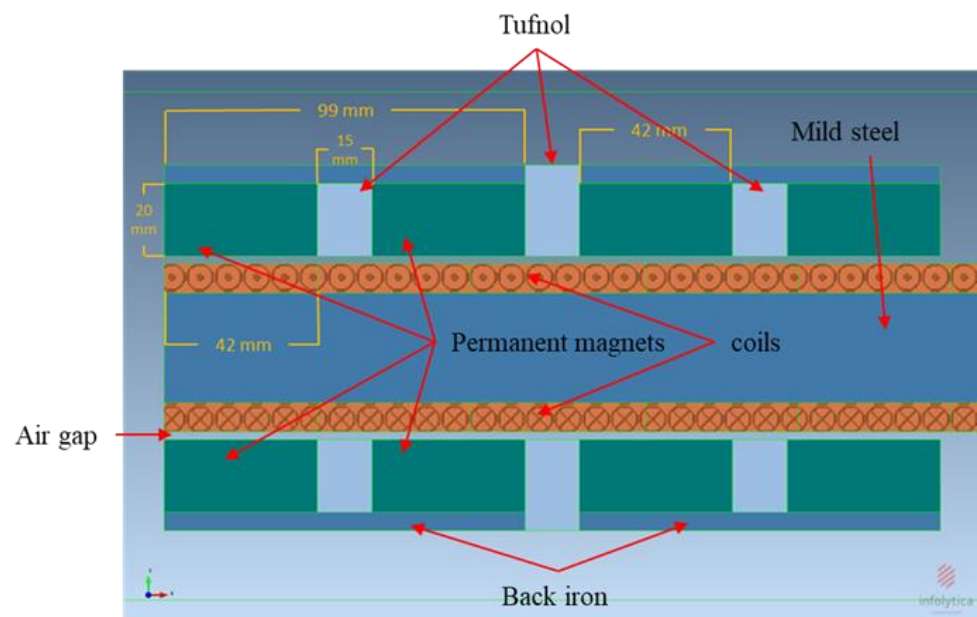


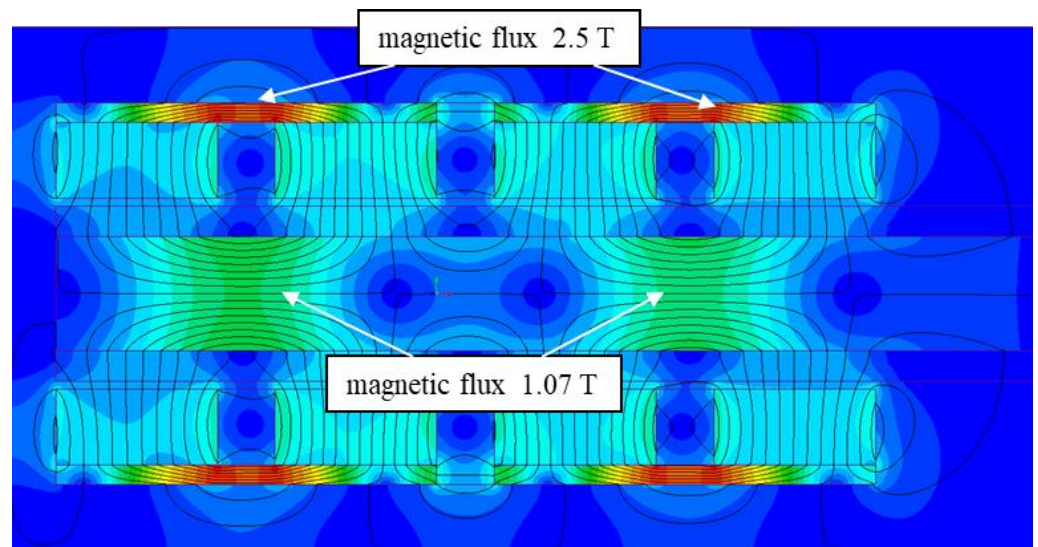
**Figure 1.** Layout of the proposed DC linear stepper motor.

**Table 1.** Dimensions and material specifications of the linear DC motor.

Name	Dimensions and Material
Magnet dimensions [mm]	42 × 20 × 30
Magnet type	Neodymium Iron Boron
Number of magnets	8
Core dimension [mm]	288 × 30 × 30
Core	Mild steel
Back iron dimension [mm]	99 × 30 × 5
Tufinol dimensions [mm]	15 × 30 × 20
Effective Air gap [mm]	10
Supply Current [A]	3

The DC linear stepper motor (DLSM) was created utilizing the finite element method (FEM). Several DLSM models with distinct structural parameters were developed, and the finest model was chosen. To validate the computing results, the optimal (DLSM) model was constructed, and its static thrust characteristics were measured. The static thrust characteristics obtained from the experimental measurements were compared to the results obtained from the simulation, and a significant level of agreement was observed between the two sets of data.

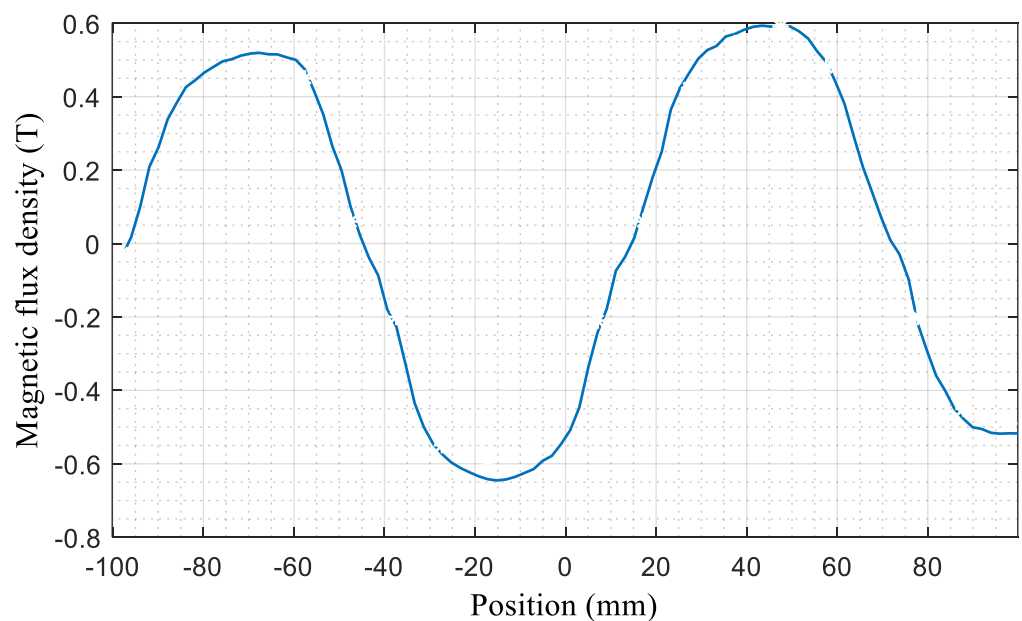
To examine the static characteristics of thrust force and air-gap magnetic flux density, accounting for the nonlinear properties of iron materials, a two-dimensional finite element method (FEM) was utilized using the “MagNet” software. The analysis focuses on the DC current excitation condition. Magnetic flux, a critical parameter for evaluating the performance of electrical machines, is of particular interest. Figure 2 illustrates the distribution of magnetic flux density across the entire cross-section of the motor and the adjacent air gap, with the lines indicating the direction of the flux. Most of the magnetic flux is concentrated at the back iron, reaching a value of 2.5 T, while the armature core exhibits a flux density of approximately 1.07 T.



**Figure 2.** Magnetic vector potential distribution throughout the cross-section of the motor.

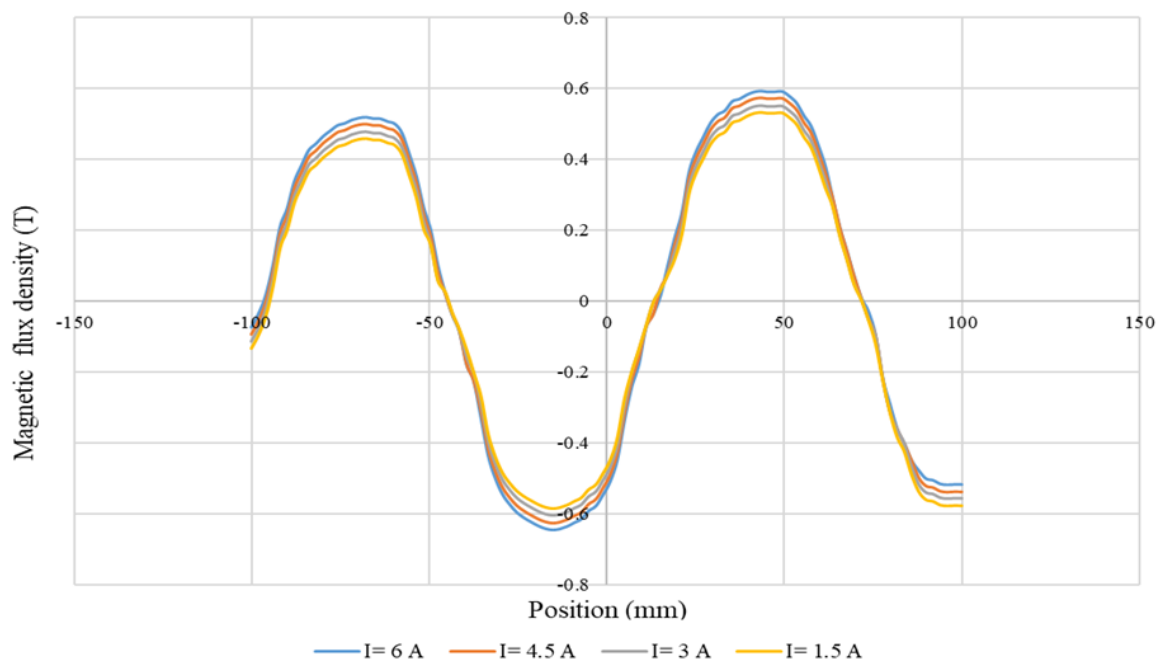
Figure 2 depicts a graph displaying the distribution of the magnetic direction potential across the cross-section of the motor and the surrounding airspace. where the red color describes a high magnetic flux density and green medium and blue low magnetic flux density. It is evident from the illustration that there are three distinct components of the leakage field originating from the moving unit. These components include the leakage field generated by the edges of the moving unit, the leakage field across the inter-polar space that separates the opposite magnet, and the leakage field emitted by the yoke. Notably, the area between the two opposing magnets produces the most significant leakage flux.

Figure 3 presents the graphs of the y-component of magnetic flux density vector in the air gap between the armature winding and the magnet. In the region of the coils, the distribution of the y-component of the magnetic flux density vector presented a shape very close to sinusoidal behavior. As can be seen from Figure 3, the peak radial flux density in the airgap occurs in the area opposite to the center of the magnet, whereas radial flux density becomes almost zero in the area opposite the space between the two magnets.



**Figure 3.** Magnetic flux density (T) in airgap.

The relationship curve of thrust with a position under different currents can be seen in Figure 4, where the magnetic flux density increased marginally as the current increased.



**Figure 4.** Magnetic flux density in airgap with different currents.

### 3. Experimental Results

The top and side view of the linear DC motor model prototype are presented as shown in Figure 5. The motor is designed to be a double-sided (U sharp) moving permanent magnet. The field system was mounted inside the carriage and installed on aluminum rails with linear bearings parallel to the armature length to guide its movement. In this model, the air gap is designed to be adjustable to study the effect of the change in the air gap on the thrust of the motor.



(a) Top view



(b) Side view

**Figure 5.** The proposed linear DC motor.

The mover component was a permanent magnet installed inside the carriage that represented the field system. Figure 6 depicts the simulation and real-time setup of a permanent magnet moving unit.

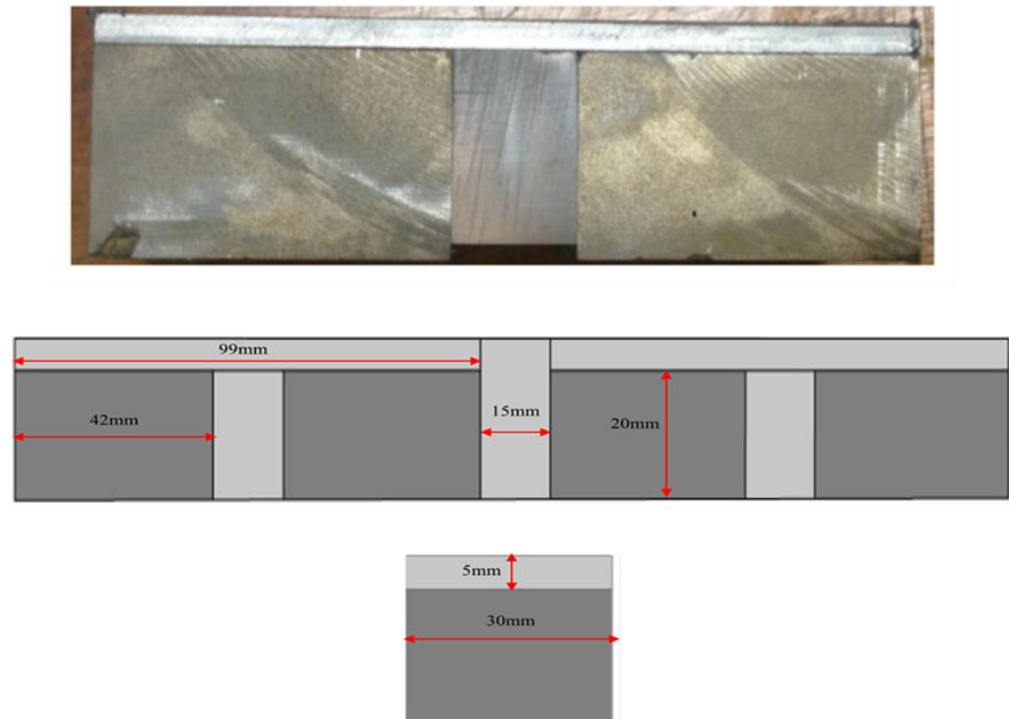


**Figure 6.** Configuration of permanent magnet moving unit.

The design of the armature windings for the motor considered various factors such as the power requirements, current carrying capability, and the desired track length. The armature core was constructed using a mild steel bar measuring 1.2 m in length with a cross-sectional area of 25 mm × 25 mm. This design determines the total distance the motor can travel along its track.

The armature windings were distributed along the armature core, as illustrated in Figure 7. There are 28 separate multi-layer coil sections evenly spaced out along the core. These coil sections are constructed using enameled copper wire with a diameter of 0.5 mm, which is equivalent to the size of 24 AWG wire. This wire size allows for a maximum direct current (DC) of 29 A to flow through the windings.

In the design of the armature windings, the diameter of the wire plays a crucial role. A smaller wire diameter allows for a greater number of turns per meter of length in a given section of the armature winding. This, in turn, leads to an increase in the force produced by the motor. However, it is important to note that as the wire diameter decreases, the current carrying capability of the wire also reduces.

To facilitate the connection of the armature windings to the power supply, connector blocks were fixed to a rail positioned directly above the armature. These connector blocks are linked to the power supply through switching circuits, enabling the controlled application of electrical current to the armature windings.

During the winding process, the armature windings are manually wrapped around the armature core, which has dimensions of 30 mm × 30 mm × 42 mm. Each individual coil section comprises 670 turns and is supplied with a direct current (DC). To achieve commutation, the armature sections are energized in a specific sequence, facilitated by a microcontroller.

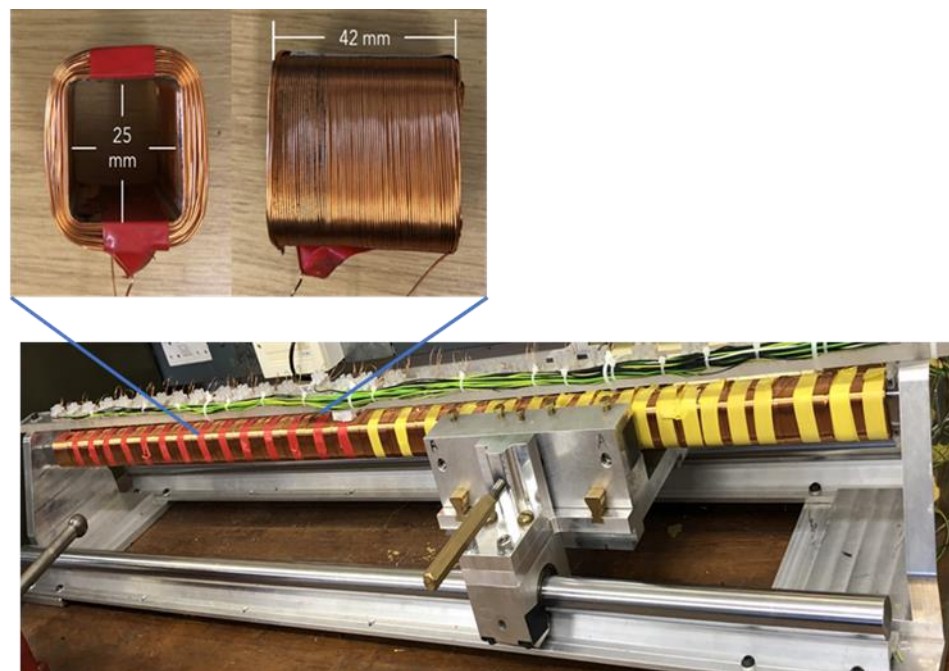


**Figure 7.** Configuration of the winding.

A model of the linear motor depicted in Figure 3 was constructed, and its measurement of thrust forces helped to validate the analytical model. For the experimental portion of the investigation, a test apparatus was built. Using a load cell (force sensor), measurements of forces in static conditions were obtained. Calibrated with ( $1 \text{ mV} = 12.51 \text{ N}$ ), the output voltage of the load cell is linearly proportional to the applied load. The sensitivity of the load cell is  $2 \text{ mV}$ . Figure 8 depicts the apparatus used to measure thrust force. During the experiments, a current was only supplied to three coils located beneath permanent magnets with normal magnetization.

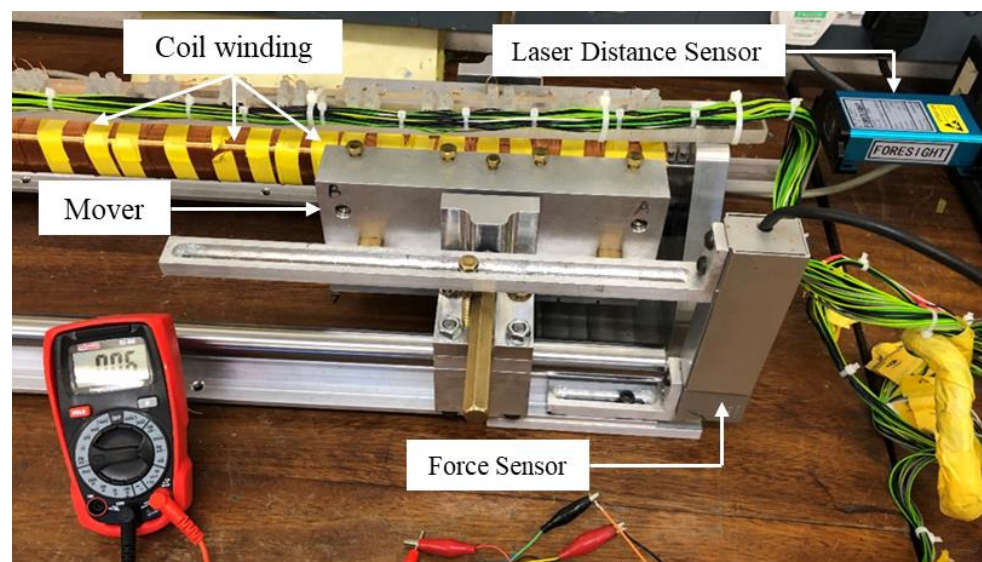


**Figure 8.** Measurement of static thrust.

The results were measured under the same current and position circumstances as in the analytical technique in order to compare and validate the simulation model. The Gaussmeter “Lakeshore 480” was used to acquire the measured values. A sinusoidal pattern may be seen in the magnetic flux density’s behavior. The findings of the magnetic

flux density vector, as shown in Figure 4, reveal a discrepancy of 7.14% between the peak values that were predicted and those that were observed.

Utilizing Equations (2) and (3), we can determine the thrust force by calibrating the load cell output, which corresponds to 1 mV, equaling 12.51 N. The load cell's output voltage was measured to be 7.6 mV when a current of 2 A was applied to each of the three coils.

The total force was calculated to be  $F = 95.07$  (N), where the static force  $k_t$  of the DLSM is calculated as 16.88 (N/A), where:

$L = 42$  mm length of the coil;

$N = 670$  number of turns;

$B = 0.6$  flux density in airgap.

In Figure 9, a comparison is presented between the experimental and computed static thrust, as the armature current is changed. A percentage error exists between the slopes of the simulated and measured values of the static thrust. This disparity can be attributed to factors such as the frictional force, leakage field and normal force resulting from the unbalanced force of attraction between the armature core and magnetic poles on either side of the motor.

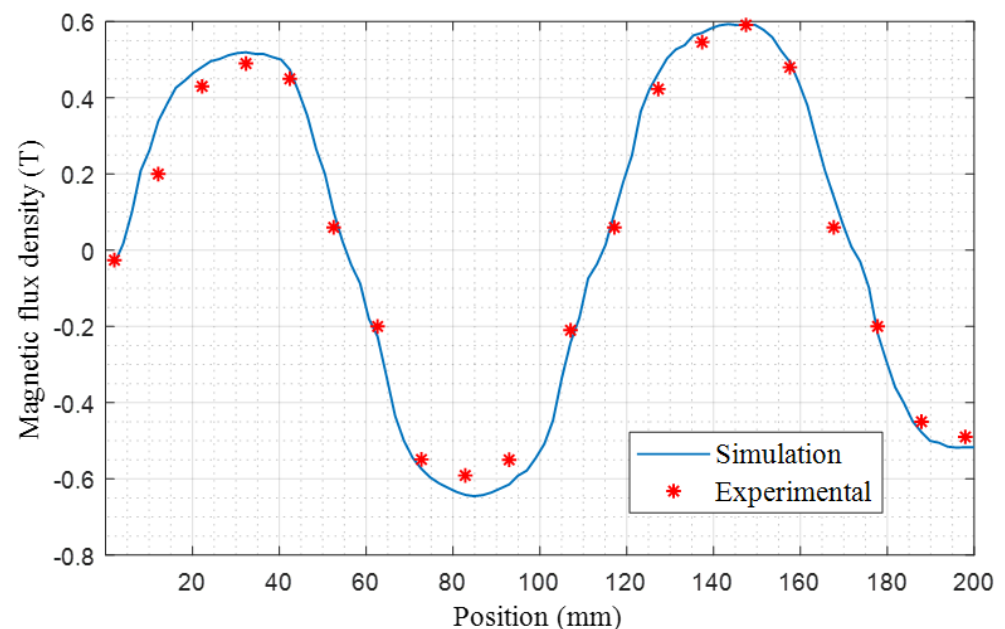
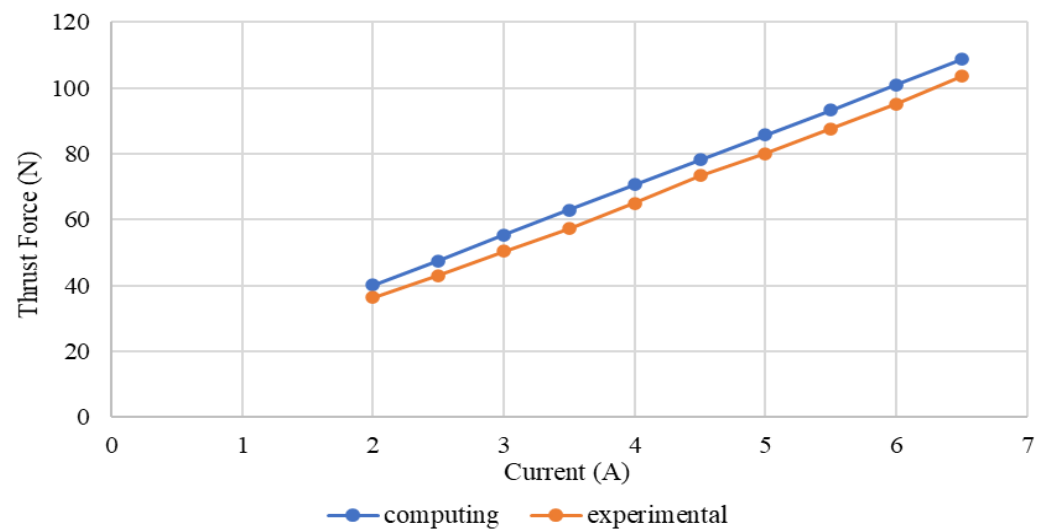


Figure 9. Measurement and simulate results of the flux density in airgap T.

The results indicate a good agreement between the measured and computed values, with the static thrust being directly proportional to the excitation current as can be seen in Figure 10. From the obtained results, it can be observed that the maximum deviation between the computed and measured data amounts to 8.07%.

The present study also assisted in analyzing the behavior of the motor's developed thrust force as a function of the air-gap length. Figure 11 depicts the thrust force as a function of various air-gap lengths when the coil current under the permanent magnets with normal magnetization is 6 A.

It can be observed that thrust decreases as airgap increases. Due to the mechanical restriction guidance of the moving unit, a minimum airgap of 6 mm, which represents the mechanical clearance between the armature winding and the moving magnets, was chosen for this model. Figure 6 shows the behavior of the thrust force in relation to the airgap length. The difference in the developed propulsion between the simulated and measured values is 5.02%.



**Figure 10.** Comparison between the experimental and simulation static thrusts.

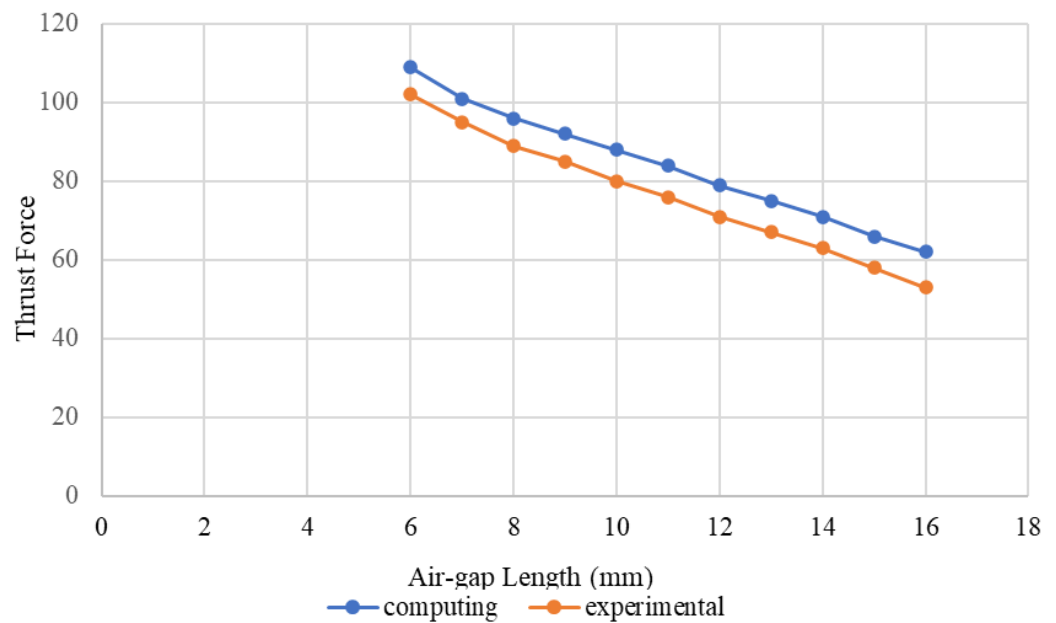


**Figure 11.** Thrust force with different airgap length values.

The parameters of the modelling linear DC motor are listed in Table 2.

**Table 2.** Parameters of the proposed DC linear stepper motor.

Parameters	Symbol	Value
Armature resistance	$R$	$7 \Omega$
Armature inductance	$L$	1.17 mH
Mover mass	$M$	7.9 kg
Thrust constant	$k_f$	16.88 N/A

#### 4. Conclusions

In conclusion, this paper concentrated on the design and modelling of a DC linear stepper motor (DLSM) to investigate its static characteristics, including thrust force and air-gap magnetic flux density. The analysis considers the nonlinear properties of the utilized iron materials. To accomplish this, a Finite Element Method (FEM) analysis using “MagNet” software was utilized to construct and model the (DLSM). The results of the

simulation were compared to actual measurements of thrust force, air-gap flux density, and static thrust force at various air gaps. By incorporating the nonlinear properties of the iron materials and employing FEM, this study provides valuable insights into the static performance of the DLSM and validates the simulation results' accuracy by comparing them to experimental measurements.

The distribution of the y-component of the magnetic flux density vector in the air gap was sinusoidal, with maximal values occurring opposite to the magnet's center. The maximal values of experimental magnetic flux density measurements and simulated values differ by 7.14 percent. The experimental and calculated static thrusts were in reasonable agreement, with a maximal deviation of 8.07 percent. Variations in static thrust were attributed to factors such as leakage field, frictional force, and an unbalanced force of attraction.

Furthermore, the effect of air gap length on thrust force is studied. It was observed that thrust decreased as the air gap length increased, and a minimum air gap length of 6 mm was chosen due to mechanical constraints. The thrust force exhibited a nonlinear response to the change in air gap length, and the difference between the computed and measured values was 5.02%.

Experimental measurements and simulations validate the linear motor prototype's analytical model. The study offers important insights into the magnetic flux distribution, thrust force characteristics, and consequence of air gap length on motor performance.

## 5. Future Work

In their future work, the authors aim to enhance the performance of the motor and reduce force ripple through several research directions. Specifically, they plan to implement a sliding mode control method to mitigate force ripple, leveraging the robustness of this control approach against parameter variations and external disturbances.

1. To address practical issues such as friction and force ripple disturbances, the authors will employ a disturbance observer in conjunction with the control method. This observer will estimate and compensate for the disturbances, enabling the more precise tracking of desired motor behavior.
2. Furthermore, the authors will utilize an optimization algorithm to fine-tune the control parameters. This optimization process aims to improve the overall performance of the control method by finding optimal parameter values that minimize force ripple and enhance motor performance.
3. By combining a sliding mode control, disturbance estimation, and parameter optimization, the authors anticipate that a superior control performance will be achieved for the motor, reducing force ripple, and addressing the practical challenges related to friction and disturbances.

**Author Contributions:** Conceptualization, M.H. and F.A.; methodology, M.H.; software, M.H. and K.A.; validation, M.H., F.A. and Y.X.; data curation, M.H., F.A., Y.X. and K.A., writing—review and editing; M.H., F.A., Y.X. and K.A. supervision, F.A. and Y.X., project administration, M.H. and F.A. All authors have read and agreed to the published version of the manuscript.

**Funding:** This article is part of Monier Habil's PhD dissertation, which was supported by the Libyan Ministry of Higher Education and Scientific Research.

**Data Availability Statement:** Not applicable.

**Acknowledgments:** The authors would like to acknowledge Cardiff University/School of Engineering/Wolfson Centre for Magnetics for paying the APC for the publication of this paper.

**Conflicts of Interest:** The authors declare no conflict of interest.

## References

1. Filho, N.F.B. Numerical and experimental analysis on the planar force and the magnetic field in a DC Linear Stepper Motor. In Proceedings of the 2013 Brazilian Power Electron. Conference COBEP 2013, Gramado, Brazil, 27–31 October 2013; pp. 884–889. [CrossRef]
2. Ismael, A. Microprocessor-Controlled Brushless DC linear Stepping Motor. Cardiff University, 2018. [Online]. Available online: <http://orca.cf.ac.uk/id/eprint/119080> (accessed on 5 April 2023).
3. Saadha, A.; Aravind, C.V.; Krishna, P.; Azhar, F. Analysis of taper width variations in linear reluctance machine. *J. Eng. Sci. Technol.* **2018**, *13*, 17–26.
4. Imen, S.J.; Shakeri, M. Feed forward adaptive control of a linear brushless DC motor. In Proceedings of the SICE Annual Conference, Takamatsu, Japan, 17–20 September 2007; pp. 2200–2204. [CrossRef]
5. Zhang, W.; Zhang, H.; Mu, J.; Wang, S. Design of a Single-Sided, Coreless, Flat-Type Linear Voice Coil Motor. *Actuators* **2023**, *12*, 77. [CrossRef]
6. Shahraky, A.M.; Sheikhkanloy, S.; Torkaman, H.; Toulabi, M.S. Design and Performance Prediction of a Novel Linear Switched Reluctance Motor. *Electr. Power Components Syst.* **2021**, *49*, 171–183. [CrossRef]
7. Norhisam, M.; Ezril, H.; Senan, M.; Mariun, N.; Wakiwaka, H.; Nirei, M. Positioning system for sensor less linear DC motor. In Proceedings of the First International Power & Energy Conference (PECon 2006), Putrajaya, Malaysia, 28–29 November 2006; pp. 476–481. [CrossRef]
8. Okonkwo, R. Design and performance of permanent-magnet DC linear motors. *IEEE Trans. Magn.* **2006**, *42*, 2179–2183. [CrossRef]
9. Boldea, I.; Nasar, S. Linear electric actuators and generators. *IEEE Trans. Energy Convers.* **1999**, *14*, 712–717. [CrossRef]
10. Zhang, D.; Kong, C.; Chen, Y. Modeling and Precision Control of Permanent Magnet Linear Motors. *IFAC* **2008**, *41*, 2258–2263. [CrossRef]
11. Palka, R.; Woronowicz, K. Linear Induction Motors in Transportation Systems. *Energies* **2021**, *14*, 2549. [CrossRef]
12. Murty, V.S.; Jain, S.; Ojha, A. Linear switched reluctance motor for traction propulsion system using configuration of electric locomotive. *Mechatronics* **2023**, *89*, 102916. [CrossRef]
13. Jafari, R.; Asef, P.; Ardebili, M.; Derakhshani, M.M. Linear Permanent Magnet Vernier Generators for Wave Energy Applications: Analysis, Challenges, and Opportunities. *Sustainability* **2022**, *14*, 10912. [CrossRef]
14. Zou, Y.; Cheng, K.W.E. Design and Optimization of a Homopolar Permanent-Magnet Linear Tubular Motor Equipped With the E-Core Stator. *IEEE Access* **2019**, *7*, 134514–134524. [CrossRef]
15. Chen, X.; Jiang, H.; Li, Z.; Liang, K. Modelling and Measurement of a Moving Magnet Linear Motor for Linear Compressor. *Energies* **2020**, *13*, 4030. [CrossRef]
16. Liang, K.; Stone, R.; Hancock, W.; Dadd, M.; Bailey, P. Comparison between a crank-drive reciprocating compressor and a novel oil-free linear compressor. *Int. J. Refrig.* **2014**, *45*, 25–34. [CrossRef]
17. Redlich, R.; Unger, R.; Van der Walt, N. Linear motors: Motor configuration, modulation and systems. In Proceedings of the International Compressor Engineering Conference at Purdue University, West Lafayette, IN, USA, 23–26 July 1996.
18. Tiegna, H.; Amara, Y.; Barakat, G. Overview of analytical models of permanent magnet electrical machines for analysis and design purposes. *Math. Comput. Simul.* **2013**, *90*, 162–177. [CrossRef]
19. Yan, L.; Zhang, L.; Wang, T.; Jiao, Z. Magnetic flux field analysis of slotless PM linear machine with multiple tubular movers. *Int. J. Appl. Electromagn. Mech.* **2017**, *53*, 685–695. [CrossRef]
20. Jiang, Z.; Park, J.; Xu, D.; Hwang, S. Analysis Method Development of Hybrid Linear Motor Considering Cogging Force Effect. *Actuators* **2023**, *12*, 99. [CrossRef]
21. Jiang, H.; Liang, K.; Li, Z. Characteristics of a novel moving magnet linear motor for linear compressor. *Mech. Syst. Signal Process.* **2018**, *121*, 828–840. [CrossRef]
22. Abdalla, I.I.; Ibrahim, T.; Nor, N.B.M. Development and optimization of a moving-magnet tubular linear permanent magnet motor for use in a reciprocating compressor of household refrigerators. *Int. J. Electr. Power Energy Syst.* **2016**, *77*, 263–270. [CrossRef]
23. Wang, C.; Shen, J.; Wang, L.; Wang, K. A novel permanent magnet flux-switching linear motor. *IET Conf. Publ.* **2008**, *47*, 116–119. [CrossRef]
24. Basak, A.; Anayi, F.J. A DC linear motor with a square armature. *IEEE Trans. Energy Convers.* **1995**, *10*, 462–469. [CrossRef]
25. Norhisam, M.; Azita, A.; Syed, J.; Mariun, N.; Hiram, Y. Thrust density characteristics of linear DC motor. *Proc. Int. Conf. Power Electron. Drive Syst.* **2005**, *2*, 1408–1412. [CrossRef]
26. Mizuno, T.; Iwadare, M.; Nanahara, M.; Koyama, K.; Anzai, T.; Nirei, M.; Yamada, H. Considerations on electrical and mechanical time constants of a moving-magnet-type linear DC motor. *Sens. Actuators A Phys.* **2000**, *81*, 301–304. [CrossRef]
27. Hondts, L.; Meyer, K.H. Linear dc Motor with Permanent Magnets. *Philips Tech. Rev.* **1982**, *40*, 329–337.
28. Yajima, H.; Wakiwaka, H.; Minegishi, K.; Fujiwara, N.; Tamura, K. Design of linear DC motor for high-speed positioning. *Sensors Actuators A Phys.* **2000**, *81*, 281–284. [CrossRef]
29. Song, J.; Dong, F.; Zhao, J.; Lu, S.; Li, L.; Pan, Z. A New Design Optimization Method for Permanent Magnet Synchronous Linear Motors. *Energies* **2016**, *9*, 992. [CrossRef]

30. Wróblewski, A.; Krot, P.; Zimroz, R.; Mayer, T.; Peltola, J. Review of Linear Electric Motor Hammers—An Energy-Saving and Eco-Friendly Solution in Industry. *Energies* **2023**, *16*, 959. [[CrossRef](#)]
31. Ustun, O.; Kivanc, O.C.; Mokukcu, M.S. A Linear Brushless Direct Current Motor Design Approach for Seismic Shake Tables. *Appl. Sci.* **2020**, *10*, 7618. [[CrossRef](#)]

**Disclaimer/Publisher’s Note:** The statements, opinions and data contained in all publications are solely those of the individual author(s) and contributor(s) and not of MDPI and/or the editor(s). MDPI and/or the editor(s) disclaim responsibility for any injury to people or property resulting from any ideas, methods, instructions or products referred to in the content.